APPLICATION OF SOLAR HEATING SYSTEM IN HIGH-TECH ENTERPRISES UNDER THE PHOTOVOLTAIC INDUSTRY CHAIN

by

Yixiang SUN[a*] and Nana GENG[b]

[a] Nanjing University of Aeronautics and Astronautics, Nanjing, China
[b] Nanjing University of Posts and Telecommunications, Nanjing, China

Original scientific paper
https://doi.org/10.2298/TSCI2104021S

This article designs a simple experimental training platform for high-tech enterprises to charge solar photovoltaic power generation lead-acid batteries. The platform comprises photovoltaic panels, charge controllers, valve-regulated lead batteries, and varistor box loads, indicating that the solar photovoltaic industry is high-tech, the scope and significance of application in technology companies. On this basis, the article replaces the first-order derivation with approximate gradient calculation and proposes a variable-step voltage disturbance observation method to realize the maximum power point tracking of solar photovoltaic power generation. The simple experimental training platform for high-tech solar photovoltaic power generation lead-acid batteries uses STM8S105 single-chip micro-computer as the controller core while adopting the Buck DC step-down chopper primary circuit, combined with the lead-acid battery four-stage charging method, for system hardware and software design. The experimental test shows that the experimental training platform has maximum power point tracking function, low cost, simple structure, good performance, easy operation, and maintenance, and can meet high-tech enterprises' experimental training requirements.

Key words*: photovoltaic power generation, disturbance observation method, maximum power point tracking, lead-acid battery charging*

Introduction

The use of solar energy to achieve photovoltaic (PV) power generation originated in the 1970's in the 20^{th} century, and now PV power generation systems have been installed worldwide. This system is mostly concentrated in communications, traffic signals, and power supply in remote areas. Most of these systems are relatively independent PV power generation systems. An independent PV power generation system must be equipped with a relatively complex energy storage system, which has excellent application restrictions. The PV grid-connected power generation does not require a complex energy storage system to save investment and improve the reliability of power supply. Solar energy is rich, widely distributed, and environmentally friendly. It is the most promising RES in the 2^{st} century. The full development and utilization of solar energy is an effective countermeasure to solve the energy crisis and environmental protection. A PV power generation is a form of power generation that directly converts

* Corresponding author, e-mail: sunyixiangnuaa@126.com

solar energy into electrical energy. Solar PV power generation maximum power point tracking (MPPT) is a critical teaching content for high-tech enterprises in the PV industry. However, in the experimental training process of high-tech enterprises, most of the current integrated PV power generation system experimental equipment is expensive, complicated in structure, diverse in functions, low in flexibility, and high in system operation and maintenance costs. Therefore, it is necessary to develop experimental training platforms for PV power generation high- tech enterprises with low cost, simple structure, easy maintenance, and MPPT function.

Some scholars have also proposed gradient calculation methods, improved disturbance observation methods, variable step-length disturbance observation methods, power prediction methods*, etc*. Still, most of these improved methods are simulation studies, and they are rarely used in experimental training platforms. In PV power generation systems, lead storage batteries' charging methods include direct charging, constant voltage charging, and constant current charging [1]. Besides, scholars have also proposed a variable current charging method that can predict the maximum current. A fuzzy immune algorithm staged charging method, a four-stage charging method based on UC3909 and supercapacitors, and a four-stage charging based on the intelligent disturbance observation method MPPT. However, the aforementioned control strategies are complex, require high hardware performance, and high system implementation costs.

This paper proposes an MPPT control strategy based on the approximate gradient variable step length perturbation observation method. Using the STM8S105 micro-controller and CN3717 battery charging management chip, a smart solar charger is designed, composed of PV panels, lead storage batteries, and varistor box loads. Experimental training platform for high-tech enterprises of the solar PV power generation system.

Solar power system

The solar power system's overall schematic diagram with a PV grid-connected to the distribution network is presented in fig. 1. The structure of the solar power generation system where the PV grid is connected to the distribution network includes PV arrays and integrated frames, inverter units VSR, DC power distribution units, metering units, AC power distribution units and safety protection system, as well as discharge modules and system power, supplies circuit, *etc*. The inverter unit, metering unit, AC power distribution unit, and safety protection system in the picture are all installed in a vertical cabinet. The system uses 13 strings and nine parallels, a total of 117 solar module arrays. The final modules are connected to the three-phase grid with three independent single-phase grid-connected inverter systems. The rated power of each solar module is 85 W. The advantage of this design is that the power generation system is easy to maintain, and the reliability of the system operation is high. Even if one phase fails, the other two-phases can continue to generate power. The PV array's orientation and elevation angles in the picture are 45° and 15° south and west. In designing a solar power generation system with a PV grid-connected to the distribution network, its overall structure includes many subsystems or modules, which play an essential role in the solar power system's overall operation. These subsystems are described in detail below.

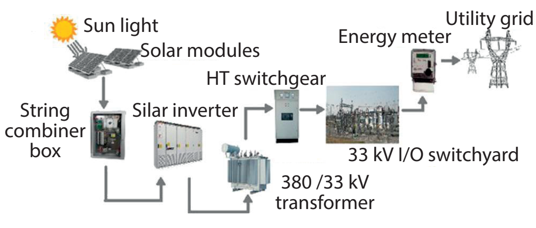

Figure 1. Grid-connected solar PV power generation system structure

The primary circuit of the solar power generation system

The solar power generation circuit in fig. 2 adopts a three-phase bridge structure, in which the voltage is connected to the grid by inductance to realize the grid-connected operation of the PV system. The frequency and phase of the sine wave current output by the device are the same as the frequency and phase of the grid voltage, and the current size of the power supply is determined according to the power output by the photovoltaic array.

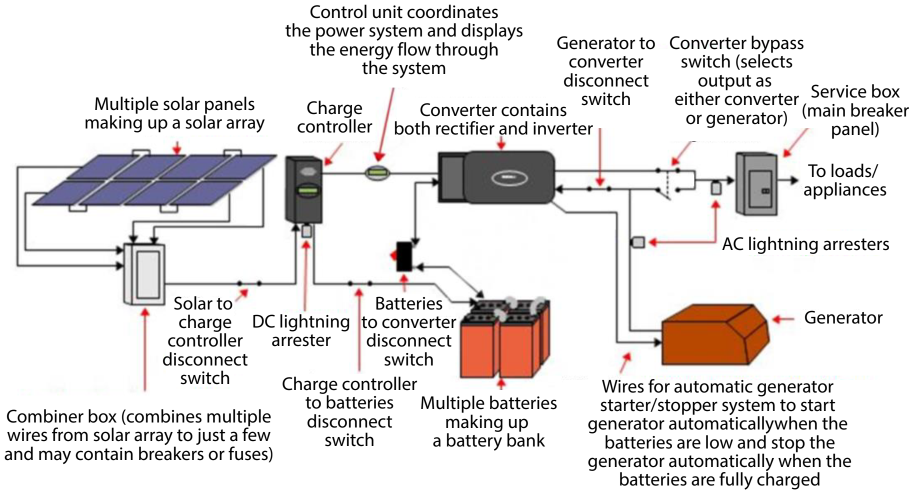

Figure 2. The primary circuit of the solar power system

Design of temperature sampling module for solar power generation system

In designing the temperature sampling module of the solar power generation system, the temperature sensor AD590 is used. According to this sensor, the power generation system's temperature is collected to ensure that the solar power generation system connected to the PV grid-connected to the distribution network operates better. For the sensor AD590, if the collected temperature is T, the current through the sensor is $I_r = AT$ where A represents the conversion coefficient, in general, $A = 1$ μA/K, the voltage at the in-phase output of the LM358 chip is: $u_p = I_r \times R_{28}$, and the voltage at the inverted output of the LM358 chip is: $u_N = V_{CC}/(R_{21} + R_{22} + R_{23} + R_{24})R_{24}$, therefore, $u_0 = (u_N - u_p) \times A_f$. Among them, A_f is the amplifying gain of the amplifying operation circuit. According to the previous parameters, the power generation system's temperature sampling module can better perform self-maintenance.

The solar power generation system's discharge control module uses TLP250 to drive the Power MOSFET as a switching device in the system's charging and discharging module. The system's charge and discharge modules are roughly similar, and the discharge control module is represented here. In the discharge module circuit in the figure mentioned previously, the Power MOSFETIRF3205 produced by IR is selected as the discharge control switch tube. When MSP430 gives a high level, Q5 turns on. The TLP250 outputs a high level, and the IRF3205 gate-source voltage is clamped at 10 V. At this time, the MOSFET is turned on, and the discharge module supplies power to the load. On the contrary, when the discharge control terminal sends out a low level, Q5 is turned off, the IRF3205 gate-source voltage will be less than the threshold voltage, and the MOSFET cannot be turned on, which is equivalent to a control switch In the disconnected state, the discharge module cannot supply power to the load.

Four-stage charging of lead-acid batteries

Because of its low price, compact structure, long service life, and maintenance-free advantages, lead batteries are often used as energy storage equipment for photovoltaic power generation. However, battery overcharging, over-discharging, and long-term floating charging will seriously affect its life. Therefore, the charger's design must refer to the characteristic charging curve and adopt a scientific charging strategy to limit the battery's charging conditions and methods. At present, lead-acid batteries generally use three-stage charging, that is, first constant current charging, then constant voltage charging, and finally floating charging. However, because the battery may be over-discharged, if the constant current charging is performed initially, it will generate heat rapidly due to the excessive charging current and burn the battery. Therefore, a small current trickle charge should be used first [2]. The domestic consonance company's battery charge management chip CN3717 is a PWM step-down mode lead-acid battery charge management integrated circuit. It has the function of TI's UC3909 chip. It is cheaper and more cost-effective. Its charging control curve is shown in fig. 3.

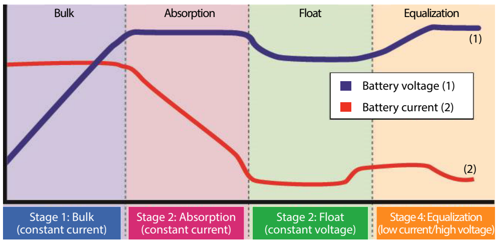

Figure 3. Four-stage charging curve of lead battery

Trickle charging stage

When the battery voltage is lower than the set threshold voltage U_T (about 81.8%U_{OC}) after the battery is over-discharged, the charger will provide a minimal charging current I_T (about 13%I_{BULK}).

Constant current charging stage

When the battery voltage is higher than U_T, the charger provides a constant high current I_{BULK} for charging, this is the main stage of charging.

Constant voltage charging stage

At this stage, the charger performs constant voltage charging U_{OC} slightly higher than the rated voltage of the battery. As the battery terminal voltage gradually increases, the current decreases exponentially until it drops to the charge termination current I_{OCT} (about 10% I_{BULK}), the charger output voltage decreases to the float voltage U_F. At this time, the battery is fully charged and enters the floating charge stage.

Floating charge stage

Keep the floating charge voltage U_F (about 93.1%U_{OC}) unchanged, and charge the battery with a small floating charge current to compensate for the capacity loss caused by the battery's self-discharge.

Approximate gradient variable step size perturbation observation method MPPT

With light intensity and temperature change, solar cells have different output volt-ampere characteristics and power-voltage characteristics. To maximize the use of solar energy and improve the PV power generation system's comprehensive conversion efficiency, we need to detect the solar panel's output voltage and load current in real-time and make the solar panel's operating point cell always near the maximum PowerPoint. This process is called MPPT.

It can be seen from fig. 4 that the *P-U* curve of a solar cell is a single-peak curve with an opening downward and continuous conduction. The vertex is the maximum PowerPoint, and the derivative of power to voltage is zero. Taking it as the boundary, it can be divided into left and right two branches [3]. The basic idea of the approximate gradient variable step disturbance observation method MPPT proposed in this paper is: adopt a smaller voltage disturbance step. This can effectively solve the contradiction between the tracking accuracy and the speed of the MPPT of the fixed-step disturbance observation method.

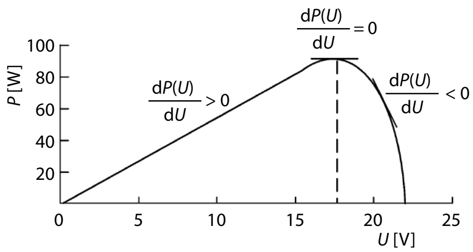

Figure 4. The *P-U* characteristic curve of solar cell

The gradient descent method is the simplest calculation method for unconstrained optimization problems based on the steepest descent method. It takes the objective function's negative gradient direction as the search direction of each iteration and gradually approaches the function's minimum value [4]. The MPPT problem can be regarded as solving the maximum value of the power *P-U* curve. Therefore, it is only necessary to change the negative gradient direction the positive gradient direction. The iterative formula for voltage disturbance:

$$U_{k+1} = U_k + ag_k \tag{1}$$

where U_k is the current working voltage and output current, U_{k+1}, I_{k+1} – the working voltage and output current of the next sampling period, respectively, α – the constant positive coefficient, g_k – the gradient value, and ag_k – the step length of the voltage disturbance, which varies with the gradient near the maximum power point. The g_k is smaller and the voltage disturbance step length is smaller, in the area far from the maximum power point, g_k is more extensive, and the voltage disturbance step length is more considerable. The gradient formula [5]:

$$g_k = \nabla P(U_k) = \left.\frac{dP(U)}{dU}\right|_{U=U_k} \tag{2}$$

where U is the PV array's output voltage, $P(U)$ – the output power function of the solar cell with U as the only variable, which is a continuous and first-order differential non-linear function. If the continuous domain derivation is expressed by the discrete domain first-order difference method, the approximate calculation of the gradient value can be expressed as eq. (3), in summary, the algorithm is shown in fig. 5:

$$g_k = \frac{U_{k+1}I_{k+1} - U_k I_k}{U_{k+1} - U_k} \tag{3}$$

Charger design

Composition of the charging control system

As shown in fig. 6, the charger is mainly composed of a PV array, a PV controller, a valve-regulated lead battery, and a power resistance load. The charge controller is composed of STM8S105S4T6C single-chip micro-computer, a large-capacity energy storage capacitor, buck DC chopper circuit, CN3717 chip, and LCD. Connect multiple sampling signals such as the solar panel's output voltage, charging voltage, charging current, and battery temperature to the single-chip micro-computer's high speed ADC module. The MCU outputs PWM pulse

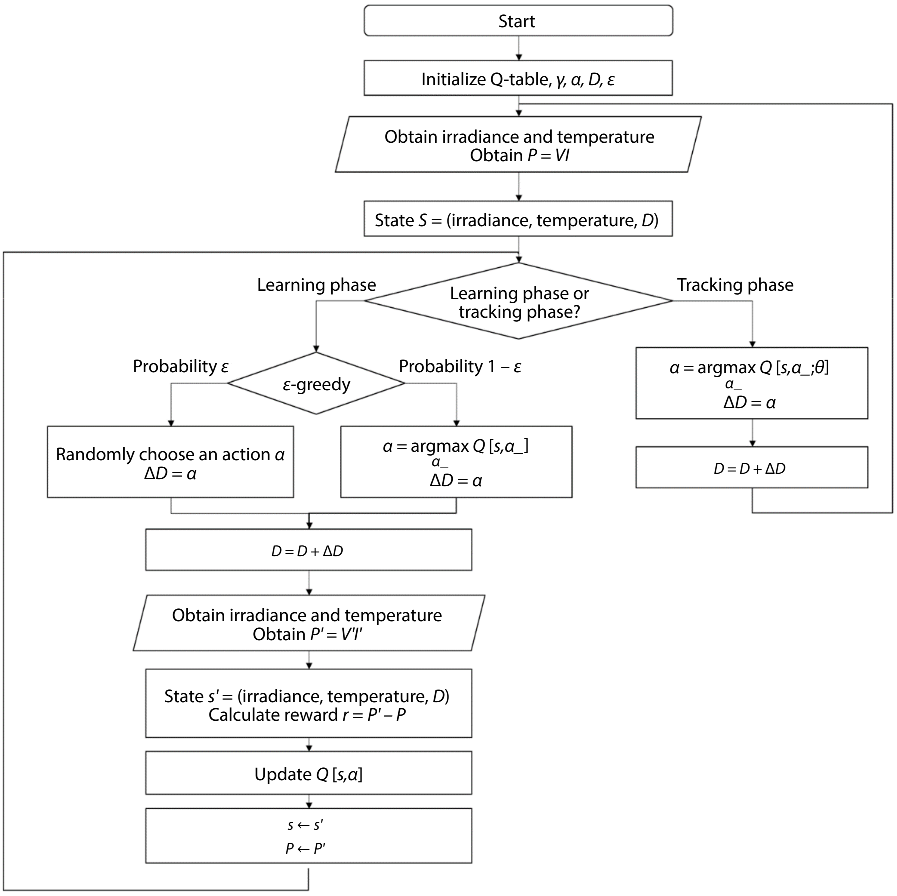

Figure 5. Flow chart of MPPT algorithm of approximate gradient variable step perturbation observation method

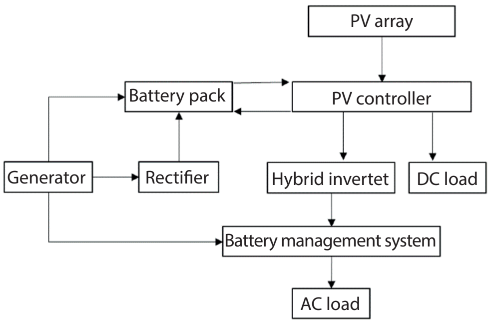

Figure 6. The composition of the solar smart charger control system

to drive the primary circuit's IGBT, stabilized by the energy storage capacitor to complete power transmission and MPPT control [6]. The single-chip micro-computer outputs the charge permission and protection signals to the chip CN3717, which outputs PWM pulses to control the PMOS tube in the Buck DC chopper circuit to realize the four-stage charging of the battery. At the same time, the MCU displays over-charge, over-discharge, charging status, power, and alarm information on the LCD.

Design of CN3717 peripheral circuit

As shown in fig. 7, the solar panel outputs a voltage of 0-18 V, which is stabilized by a large-capacity capacitor, and then through the MOSFET controlled by the single-chip micro-

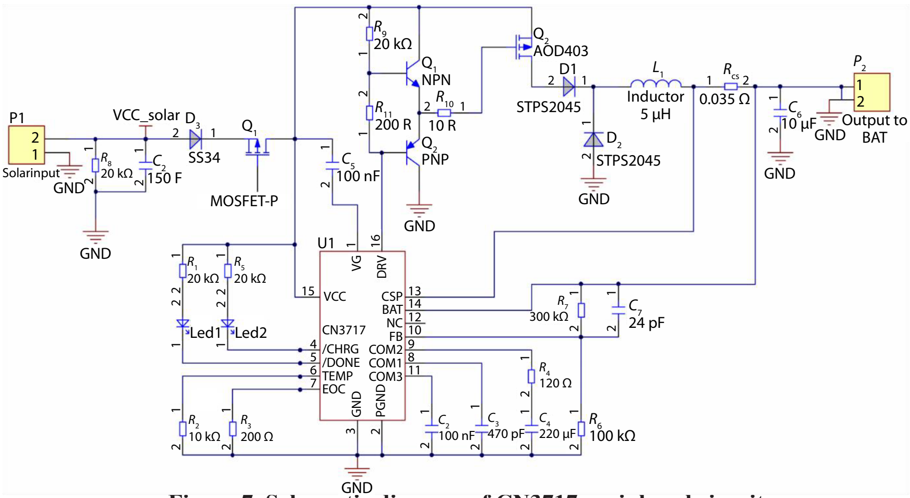

Figure 7. Schematic diagram of CN3717 peripheral circuit

computer to track the maximum power point, and then input to the controlled buck step-down chopper circuit, and finally output variable voltage to charge the battery.

According to the parameters and charging requirements of the lead-acid battery used in the project, combined with the literature data of the chip, determine the threshold voltage $U_T = 11.8$ V, trickle charging current $I_T = 0.65$ A, constant current charging current $I_{\text{BULK}} = 5$ A, and constant voltage charging voltage $U_{\text{OC}} = 14.5$ V of the lead-acid battery trickle charging, constant voltage charge termination current $I_{\text{OCT}} = 0.53$ A, floating charge voltage $U_F = 13.5$ V. Then, calculate the parameters of CN3717 peripheral circuit components [7]:

$$U_T = 3.6\left(1+\frac{R_7}{R_6}\right)+I_B R_7 \tag{4}$$

where I_B is the bias current of the F_B pin, the typical value is 40 μA. Through calculation, $R_7 = 300$ kΩ, $R_6 = 100$ kΩ, and R_{CS} is the charge current detection resistance between the CSP pin and the BAT pin:

$$I_{\text{BULK}} = \frac{175}{R_{CS}} \tag{5}$$

The R_{CE} is calculated as 35 mΩ, and constantan precision resistance is generally used. According to the formula of constant voltage charge termination current:

$$I_{\text{OCT}} = \frac{1.278(14350+R_3)}{R_{CS}\cdot 10^6} \tag{6}$$

Calculate R_3 and take 200 Ω. To make the charge controller have a high precision temperature compensation function, to monitor the lead-acid battery's temperature, a thermistor with a negative temperature coefficient –3.5 mV/°C is used between the TEMP pin and the ground, and the resistance is 10 kΩ.

Software design

In the CC Studio integrated development environment, use C^{++} to write modular programs. The main functions of each module are:

– *Initialize the module*. System preset parameter initialization, including the initialization setting of the internal integrated module register of the micro-controller.
– *Analog signal sampling and a processing module*. The PV battery output voltage and charging voltage detection, charging current sampling, lead-acid battery temperature detection, signal shaping, filtering, and A/D conversion [8].
– *The MPPT control module*. The basic algorithm includes the constant voltage method, the conductance increment method, and the disturbance observation method. The improved algorithm includes the MPPT algorithm of the variable step length approximate gradient disturbance observation method proposed in this paper. Another improved algorithm.
– *Information display module*. Display information such as charging working mode, charging status, current, voltage, power, and fault alarm.
– *Charging permission/protection module*. Complete system charging permission and over-current or over-voltage protection during charging and discharging. If the system operating parameters are abnormal, the charging or discharging circuit will be automatically cut off immediately to protect the entire circuit's load.

Experimental training platform test

The experimental training platform for high-tech enterprises in charge of PV power generation lead-acid batteries is shown in fig. 8. Among them, the model of the solar panel is SP-100, the maximum power is 100 W, the maximum output voltage is 18 V, the open-circuit voltage is 21.6 V, the short-circuit current is 5.89 A, the light intensity under ideal conditions is 1000lx, and the working temperature is 25 °C. The gel-sealed valve-regulated lead-acid battery model is NP65-12, its rated voltage is 12 V, and the battery capacity is 65 Ah. The load adopts a power rheostat box with a maximum allowable current of 13 A and a maximum resistance of 206 Ω. The main control board mainly completes signal acquisition and processing, MPPT algorithm, and LCD [9]. The charging control board controls the four-stage

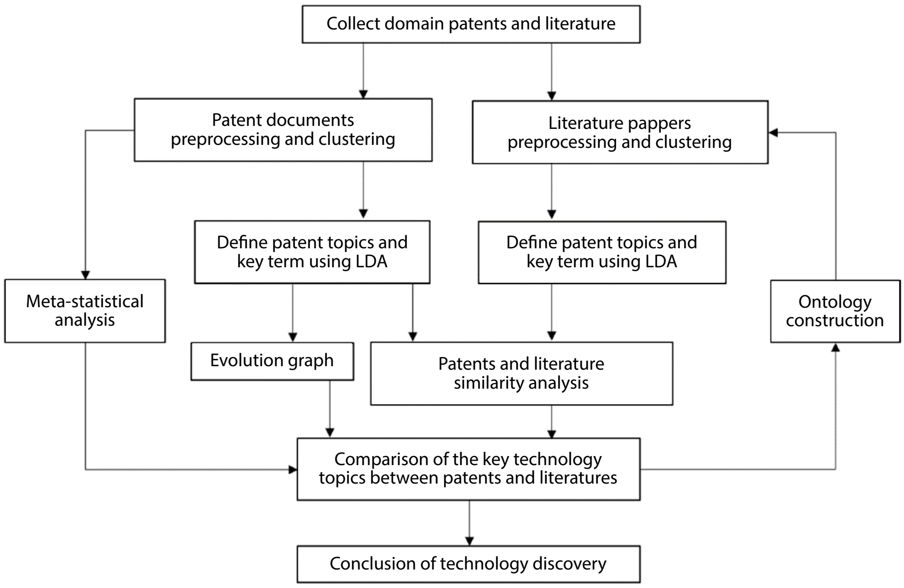

Figure 8. A simple high-tech enterprise experimental training platform for charging PV power generation lead batteries

charging process of the lead battery. Each functional unit is distributed independently, easy to overhaul, and maintain.

To monitor the whole process of charging the lead-acid battery while the experimental training platform is running, before charging, the lead-acid battery is over-discharged through the resistance box, and the voltage is 11 V. On a particular day in Guangzhou in July, from 8:00 to 19:00, the experimental training platform was used to conduct all-weather monitoring and testing. The data obtained are shown in tab. 1.

Table 1. The MPPT test of independent solar PV power generation lead battery charging system

Testing time	Battery board temperature [°C]	Light intensity [Wm^{-2}]	Light intensity [Wm^{-2}]	Battery voltage [V]
8:00	20	423	26	11.05
8:30	26	446	32	11.2
10:00	32	585	44	11.56
12:00	39	792	66	12.85
14:00	45	768	75	14.45
16:00	43	754	49	14.54
18:00	37	558	41	13.33
19:00	29	362	28	13.522
Testing time	**Charging current [A]**	**Actual output power [W]**	**Power error [%]**	**Battery power [%]**
8:00	0.62	7.2	72	4
8:30	0.66	7.4	77	6
10:00	2.23	25.8	41	15
12:00	4.92	63.5	4	38
14:00	4.87	70.5	5	77
16:00	3.13	45.4	7	91
18:00	0.55	7.1	87	94
19:00	0.48	5.4	81	93

In the floating charge stage, the floating charge voltage is limited, and the charger outputs less power to charge the lead storage battery. After 11 hours of operation, the battery is fully charged. The experimental training platform can work stably for a long time according to the preset charging parameters and usually operate, meeting high-tech enterprises' experimental training needs.

Conclusion

In response to the needs of practical training for high-tech enterprises of solar PV power generation systems, considering the safety, stability, cost-effectiveness, and prolonging the battery life of the system. Through the actual system operation test, it can be known that the MPPT algorithm can accurately track the maximum power point when the illumination continually changes, which improves the comprehensive energy efficiency of solar energy. The experimental training platform for high-tech enterprises of solar PV power generation lead-acid battery charging is of high practical value and is worthy of further research, performance optimization, and popularization and application.

Acknowledgment

This work was supported by Planning Project of Educational science of Guangdong province: *Research on spatial and temporal differentiation technology innovation of industrial agglomeration and environmental pollution decoupling of the Guangdong-Hong Kong-Macao Greater Bay Area* (2019GXJK068), Philosophy and Social Science Planning Project of Guangdong Province *Empirical Research on the Impact of Economic Development of Guangdong Province on the Ecological Environment-The Perspective of Audit Evaluation* (GD18XYJ28) and the Program for Innovative Research Team of Huizhou University.

References

[1] Elshkaki, A., Materials, Energy, Water, and Emissions Nexus Impacts on the Future Contribution of PV Solar Technologies to Global Energy Scenarios, *Scientific Reports*, *9* (2019), 1, pp. 1-19
[2] Varma, R. K., Salehi, R., The SSR Mitigation with a New Control of PV Solar Farm as STATCOM (PV-STATCOM), *IEEE Transactions on Sustainable Energy*, *8* (2017), 4, pp. 1473-1483
[3] Kumar, S. S., *et al*., Design of Evacuated Tube Solar Collector with Heat Pipe, *Materials Today: Proceedings*, *4* (2017), 14, pp. 12641-12646
[4] Koundinya, S., *et al*., Experimental Study and Comparison with the Computational Study on Cooling of PV Solar Panel Using Finned Heat Pipe Technology, *Materials Today: Proceedings*, *4* (2017), 2, pp. 2693-2700
[5] Li, C., *et al*., Engineering Graphene and TMD Based Van der Waals Heterostructures for Photovoltaic and Photoelectrochemical Solar Energy Conversion, *Chemical Society Reviews*, *47* (2018), 13, pp. 4981-5037
[6] Wu, S., Construction of Visual 3-D Fabric Reinforced Composite Thermal Perfomance Prediction System, *Thermal Science*, *23* (2019), 5, pp. 2857-2865
[7] Dehra, H., Acoustic Signal Processing and Noise Characterization Theory Via Energy Conversion in a PV Solar Wall Device with Ventilation through a Room, Advances in Science, *Technology and Engineering Systems Journal*, *3* (2018), 4, pp. 130-172
[8] Dehghani Madvar, M., *et al*., Analysis of Stakeholder Roles and the Challenges of Solar Energy Utilization in Iran, *International Journal of Low-Carbon Technologies*, *13* (2018), 4, pp. 438-451
[9] Wu, S., Study and Evaluation of Clustering Algorithm for Solubility and Thermodynamic Data of Glycerol Derivatives, *Thermal Science*, *23* (2019), 5, pp. 2867-2875

Paper submitted: November 25, 2020
Paper revised: January 9, 2021
Paper accepted: January 25, 2021